Self-Assembled DNA-PEG Bottlebrushes Enhance Antisense Activity and Pharmacokinetics of Oligonucleotides

*Yuyan Wang, Dali Wang, Fei Jia, Andrew Miller, Xuyu Tan, Peiru Chen, Lei Zhang, Hao Lu, Yang Fang, Xi Kang, Jiansong Cai, Mengqi Ren, and Ke Zhang**

Department of Chemistry and Chemical Biology, Northeastern University, Boston, Massachusetts 02115, United States

KEYWORDS: PEGylation, DNA self-assembly, antisense oligonucleotide, hybridization chain reaction, DNA nanostructures

ABSTRACT: Herein, we report a novel strategy to enhance the antisense activity and the pharmacokinetics of therapeutic oligonucleotides. Through the DNA hybridization chain reaction, DNA hairpins modified with poly(ethylene glycol) (PEG) form a bottlebrush architecture consisting of a double-stranded DNA backbone, PEG side-chains, and antisense overhangs. The assembled structure exhibits high PEG density on the surface, which suppresses unwanted interactions between the DNA and proteins (e.g. enzymatic degradation) while allowing the antisense overhang to hybridize with the mRNA target and thereby deplete target protein expression. We show that these PEGylated bottlebrushes targeting oncogenic KRAS can achieve much higher antisense efficacy compared with unassembled hairpins with or without PEGylation and can inhibit the proliferation of lung cancer cells bearing the G12C mutant KRAS

gene. Meanwhile, these structures exhibit elevated blood retention times in vivo due to the biological stealth properties of PEG and the high molecular weight of the overall assembly. Collectively, this self-assembly approach bears the characteristics of a simple, safe, yet highly translatable strategy to improve the biopharmaceutical properties of therapeutic oligonucleotides.

INTRODUCTION

Since conceptualization in 1978, antisense oligonucleotides (ASOs) have been explored as a promising therapeutic modality for treating various diseases, based on their ability to inhibit the translation of target mRNAs.[1-3] However, therapeutic ASOs have yet to fully realize a key promise of the informational drug – that drug development can be rapidly accelerated by changing the sequence of the ASO, with only ten drugs reaching the market over four decades.[4] Key technical challenges include the minimization of immune response while achieving sufficient gene depletion, stabilizing the nucleic acid against degradation, and efficient cellular and in vivo delivery.[5-6] Currently, the most successful strategy to overcome these difficulties is through the use of various chemical modifications, which greatly improve nucleic acid stability.[7-8] However, unsatisfactory protein depletion efficiency often requires large doses of these drugs, limiting the therapeutic window and the disease areas for which effective ASO agents can be developed.[9] Another solution involves the use of advanced delivery systems such as polycationic polymers, nanoparticles, and liposomal formulations, among others.[10-14] These systems, however, oftentimes introduce additional complications including carrier-associated toxicity, immunogenicity, and large-scale production issues.[15-16] To date, only the liposomal system has achieved clinical success.[17] Therefore, a safe and simple method to realize strong antisense efficacy is still very much desired.

PEGylation, referring to covalent conjugation with PEG, is a widely adopted method to elevate the biopharmaceutical properties of biologics.[18-19] Typical PEGylation involves the attachment of linear or slightly branched, high molecular weight PEG. For example, pegaptanib, a selective vascular endothelial growth factor (VEGF) antagonist, is an ASO conjugated to a 40 kDa Y-shaped PEG.[20] We and others have shown that oligonucleotide conjugates with low PEG density cannot sufficiently suppress protein access to the payload.[19, 21] For example, no apparent difference was observed in the half-lives of PEGylated and non-PEGylated DNA when they are treated with the nuclease, DNase I.[22] An alternative PEGylation strategy involves a bottlebrush-architectured PEG, which leverages steric compaction as opposed electrostatic complexation as the means for nucleic acid protection. These high-density PEG-DNA conjugates (termed pacDNA) consist of 25-35 PEG side chains of a moderate MW (5-10 kDa) and 1-5 strands of oligonucleotides attached to a central core or backbone.[23-24] The densely packed PEG chains greatly elevate steric shielding for the oligonucleotides while still allowing the embedded antisense strands to hybridize with their targets unhindered.[25] This simple yet powerful design reduces nearly all side effects (e.g. coagulopathy, immune system activation, degradation) while substantially improving plasma pharmacokinetics (PK), passive tumor targeting, and access by non-liver organs.[26] Thus, the pacDNA makes it possible to expand oligonucleotides into additional disease areas than they are typically considered for, such as oncology.

Through our previous studies of pacDNA, we have determined that DNA stability is a function of "depth" from the brush backbone; greater distance from the backbone renders the nucleotide more prone to protein access and nuclease digestion.[22] Thus, to maximize DNA stability, we rendered DNA itself as the backbone of the brush via self-assembly of DNA monomers.[27-29] While this design improves the nuclease stability and PK of the DNA, the antisense function is

lost. Herein, we introduce a new design of monomers used for hybridization chain reaction (HCR)[30-32] that incorporates antisense functionality into the DNA-backboned bottlebrush. Our design combines the antisense motif into the structure-forming domains of the DNA hairpins, which are monomers for HCR. Upon introduction of an initiator strand, the two PEGylated hairpins undergo a cascade of strand displacement reactions, resulting in a long, double-stranded DNA backbone with PEG side chains and multiple partial antisense overhangs (Schemes 1 and S1). These overhangs bind with the target mRNA once internalized by cells, which peel off a full antisense ASOs from the nanostructure, leading to target protein depletion.

RESULTS AND DISCUSSION

Typical hairpin monomers for HCR consist of three domains, a stem, a loop, and a sticky end with a total length of ~50 nucleotides (nts).[33] To incorporate antisense overhangs into the final structure, we elongated the sticky end of one of the hairpins using an ASO that bind to the 3' untranslated region of the KRAS mRNA, which addresses all mutant and wild-type KRAS isoforms.[34] An initiator oligonucleotide is added to a 1:1 mixture of the two hairpins to trigger the HCR cascade. Our initial approach was to use a set of shorter-than-usual hairpins in order to maximize the packing density of PEG side chains in the resulting brush. The two hairpins were designed with 41 or 34 nts in length, 12 nts in the stem, and 12 or 5 nts in the sticky end, respectively (Table S1). However, after dialysis into physiological buffer (phosphate buffered saline, PBS) from the synthesis buffer (sodium phosphate sodium chloride [SPSC]), the assembled structures exhibited poor stability, with only 20% of high MW fractions remaining (Figure S1). This problem reveals that the presence of the overhangs requires a longer stem region to stabilize the overall assembly. Therefore, a second set of hairpins was designed with a stem of 18 nts and an overall length of 48 or 58 nts, which resulted in a significant increase in the

yield after dialysis (~98%) (Figure S2B). The elongated antisense overhang of hairpin 2 (HP2) is 10 nts in length, with an additional antisense region (6-nt long) embedded in the stem region, for a total antisense region of 16 nts. The hairpins were also designed to incorporate a dibenzocyclcooctyne (DBCO)-modified thymine (T) base in the stem domain, which allows for conjugation to azide-modified PEG via click chemistry (Scheme S2).[35] Both the DBCO-modified hairpin and the PEGylated hairpin were purified via reversed-phase HPLC (Figure S3). Successful PEGylation was confirmed by aqueous gel permeation chromatography (GPC) and agarose gel electrophoresis (AGE, Figure S4). Both unmodified and PEGylated hairpins were able to undergo HCR as demonstrated by AGE (Figure 1A). The average degree of polymerization (DP) decreases with increasing initiator:hairpin ratio. While unmodified hairpins achieved the highest DP with 0.3 molar equiv. of the initiator, the PEGylated hairpins require 0.5 equiv. of the initiator to maximize assembly, with a yield of ~80% after purification by GPC and dialysis into PBS (Figure S2). Note that due to the dynamic nature of HCR assemblies, complete separation of HCR-assembled structures from monomers is difficult. Even after fractionation by GPC, unassembled monomers gradually appear on AGE over time. Interestingly, these nanostructures can be stored in the dry state after lyophilization. After reconstitution with PBS buffer, negligible disassembly (<5%) was observed (Figure S5).

In addition to AGE, these nanostructures were also characterized by dynamic light scattering (DLS), transmission electron microscopy (TEM), and zeta potential measurement. DLS reveals that, upon PEGylation, the volume-average hydrodynamic diameters increase from 28 ± 1 nm to 502 nm ± 90 nm (Figure S6A). These results were corroborated by TEM imaging, showing a fibrous morphology for the assembled products in the dry state, with the PEGylated version appearing more pronounced in thickness and length (Figure 1B). Such morphology is distinctly

different from that of a simple mixture of unconjugated hairpin and PEG (Figure S7). The zeta potentials appear unaffected by the assembly; the PEGylated monomers and brushes both have lower negative charge (-9.69--8.38 mV) than the unmodified structures (-26.64--19.56 mV) (Figure S6B).

To gauge the shielding effect of PEGylation and self-assembly, we investigated the in vitro stability of DNA against DNase I, an endonuclease that acts upon single- and double-stranded DNA. Purified, pre-assembled cyanine (Cy5)-labeled DNA nanostructures with or without PEGylation were incubated with DNase I (0.4 unit/ml) in assay buffer (PBS with 2.5 mM $MgCl_2$ and 0.5 mM $CaCl_2$) at 37°C. The relative amounts of high-MW fractions (>50 kDa) were stained using ethidium bromide (EB) and monitored by AGE as a function of time (Figure 1C). It was revealed that, the PEGylation can retard the degradation rate by a factor of ~2 (measured as an increase in enzymatic half-life) (Figure 1D). While this value is less than that of brush polymer-based pacDNA (10-20×), it is comparable to other DNA-stabilizing strategies such as spherical nucleic acids (typically 2-5×)[36] and DNA nanostructures (3×)[37]. The Cy5-channel exhibited the same trend of degradation as the EB channel (Figure S8), but showed the degraded fragments more clearly. Of note, the DNase I half-life values are only useful for comparison of different structures; the test condition does not represent physiological or intracellular nuclease type or concentration. In full serum (10% FBS) RPMI medium, all monomers and assemblies exhibited negligible degradation during a 24 h incubation period as revealed by AGE analysis (Figure S9), suggesting that intact structures can persist in serum long enough for them to produce a biological response.[38]

Next, we examined if self-assembly and/or PEGylation has an impact on cellular uptake of the DNA. Lung cancer cells (NCI-H358, a $KRAS^{G12C}$ mutant non-small cell lung carcinoma

[NSCLC] cell line) were treated with different doses of Cy3-labeled DNA assemblies with and without PEGylation, and the corresponding monomers in serum-free RPMI medium (Figure 2A and 2B). Surprisingly, the PEGylated hairpin monomer exhibited uncharacteristically high levels of cell-associated signals, which is ~45× higher than the assembled nanostructures based on the same monomer. The non-PEGylated hairpin monomer also resulted in higher cellular uptake compared to the assembled structure (~4×). A similar trend was also observed in PC9 cells, which is also an NSCLC cell line but with wild-type KRAS (Figure S10). One interpretation of these results is that the secondary structure of the hairpins is responsible for non-specific interaction with a membrane component, which leads to increased binding and subsequent uptake. Assembly of the hairpins removes the secondary structure, leading to a return to normal uptake levels. The PEGylated hairpins showed by far the highest rate of uptake, which is attributed to stabilization or altering of the secondary structure via a localized volume exclusion effect from the PEG.[25] To test this hypothesis, we designed a scrambled oligonucleotide with the same number of the four bases as HP2 but without the ability to form secondary structure. Indeed, the uptake for the PEGylated, scrambled strand is at the normal level expected for DNA uptake (Figure S11). While the assembled structures underwent slower uptake compared to the monomers, the level of uptake was increased by longer incubation times. After 24 h of incubation, a 7.5× increase of uptake was observed relative to the level at 4 h, as determined by flowcytometry and confocal microscopy (Figures 2 and S12). The imaging experiment was also repeated using full serum RMPI media (Figure 2C) and Cy5-labeled DNA and assemblies (to match the dye used in nuclease degradation study, *vide supra*). Similarly, unmodified and PEGylated hairpins resulted in significant signals after 4 h, while the assemblies exhibited comparable levels of Cy5 fluorescence after 24 h. The similarity of cell uptake in serum-free and

serum-containing media suggests that the DNA structures are stable during the test period and premature enzymatic degradation is not a significant factor contributing to the observed cell uptake.

The mechanism for the cell uptake of the PEGylated hairpins and assemblies was also investigated. NCI-H358 cells were pretreated with a panel of pharmacological inhibitors for 30 mins, before incubation with Cy3-labeled, PEGylated hairpin/assembly for 24 h. Pretreatment with NaN_3 reduced the uptake of PEGylated assembly and PEGylated hairpins by more than 70% (Figure S13), suggesting an energy-dependent endocytosis pathway.[39] Less than 10% reduction was observed after treatment with chlorpromazine, which excludes the clathrin-mediated endocytosis as a major uptake pathway. The PEGylated assembly group pretreated with filipin III (which inhibits lipid raft endocytosis) and fucoidan (which competitively blocks scavenger receptor) exhibits 43% and 39% reduction in cellular uptake, respectively. Similar reduction in cellular uptake for the hairpins was also observed (52% and 49%). Taken together, these results indicate that PEGylated hairpin/assembly are taken up by a similar pathway, which is energy-dependent and associated with the scavenger receptors and lipid-raft.

To evaluate the antisense efficacy and the phenotypic response of KRAS depletion on cells with mutant vs. wildtype KRAS genes, NCI-H358 and PC9 cells were treated with the DNA assemblies and controls. KRAS depletion was confirmed by western blotting analysis (Figure 3A). DNA assemblies with or without PEGylation can both effectively knock down the target expression in the two cell lines tested. At the highest dose (10 μM ASO), both resulted in ~60% knockdown, which is on a par with lipofectamine-based transfection. Dosage benefit beyond 1 μM of antisense DNA is not obvious; knockdown plateaus at around ~60% in both NCI-H358 and PC9 cell lines (Figure S14). In contrast, the monomer units exhibited no antisense activity at

the same dose, despite much higher cell uptake. These results suggest that not all cell uptake is equally productive for gene regulation; certain uptake pathways, different cell lines, stability differences, etc. may drastically change the levels of "productive uptake".[40] Although hairpin monomers (with or without PEGylation) were rapidly associated with cells, binding with specific membrane sites may result in non-productive internalization. For example, the micropinocytosis pathway was regarded as a possible non-productive pathway for unformulated ASOs.[41] The precise mechanism of the improved productive uptake for the assembled structures is to be further investigated.

Next, we investigated if downregulation of KRAS can produce a phenotypic response in cancer cells with mutant KRAS. KRAS depletion resulted in a discernible reduction in the viability of NCI-H358 cells but not PC9 cells, as determined by 3-(4,5-dimethyl-thiazol-2-yl)-2,5-diphenyl tetrazolium bromide (MTT) cytotoxicity assay (Figure 3B). Conversely, lipofectamine-based transfection of hairpin monomers bearing the same ASO sequence resulted in toxicity in both cell lines, likely a carrier-associated toxic effect. The difference in cellular response is in agreement with a recent report showing that downregulation of mutant and wild-type KRAS isoforms has selective phenotypic effects on KRAS mutant cells in terms of viability and colony formation.[34] The cell viability results were further corroborated by cell apoptosis measurements. Using fluorescein isothiocyanate-annexin V/PI staining and flow cytometry, it was revealed that NCI-H358 cells treated with PEGylated DNA assemblies exhibited the highest induction of apoptosis (22%), with the majority of the apoptosing cells in the late phase (Figure 4A). In contrast, a scrambled PEGylated DNA assembly and PBS-treated cells showed 12% and 6% of cell population in apoptosis. Collectively, these data indicate that the PEGylated bottlebrush

ASOs exhibit enhanced antisense activity and can selectively inhibit the proliferation of NSCLC cells bearing the mutant KRAS gene.

A key design feature of the PEGylated DNA nanostructures is the improved plasma PK resulting from the biological "stealth-like" nature of the PEG and the high overall molecular weight, which allows the nanostructure to evade rapid renal clearance via glomerular filtration (MWCO of ~50 kDa). A plasma PK study was performed using immunocompetent (C57BL/6) mice. Cy5-labeled hairpin and assemblies (PEGylated and non-PEGylated) were injected via the tail vein of the mice, and blood samples at various predetermined time points up to 8 hours were collected and analyzed (Figure 4B). The hairpin monomers were rapidly cleared from blood circulation with a half-life of ~5 min, while the PEGylated hairpin showed a slightly improved half-life of ~12 min, which is similar to the non-PEGylated assembly (half-life: ~17 min). The PEGylated assemblies exhibited the most prolonged retention times, with the half-life of 50 mins. This improvement represents an 8.4× increase in the blood availability (as represented by the area-under curve [AUC∞]) compared to the hairpin monomers alone (Figure 4C).

CONCLUSION

In summary, we report a programmed assembly-based method to improve the biopharmaceutical properties of therapeutic oligonucleotides. By combining PEGylation and self-assembly, a DNA-backboned bottlebrush architecture was achieved with high-density PEG side chains and antisense overhangs. While these structures undergo limited cell uptake, they exhibit far higher antisense activity compared to their constituent hairpin building blocks and can exert a specific inhibitory effect on KRAS-mutant lung cancer cells compared with lipofectamine-based transfection. In addition, consisting of only PEG and DNA, these structures

are highly biocompatible and exhibit prolonged plasma half-lives owing to their large molecular size, which allows them to evade glomerular filtration by the kidney. We anticipate that the DNA assembly-based approach will provide a safe and simple route to more effective oligonucleotide therapeutics.

EXPERIMENTAL SECTION

Procedure for hybridization chain reaction

The HP1 and HP2 (10 nmol) strands were each dissolved in 100 μL 1× SPSC buffer (1 M NaCl, 50 mM Na_2HPO_4; pH 7.5) in microcentrifuge tubes, and were heated to 95°C for 5 min, followed by slow cooling to room temperature in a thermally insulated container overnight. After the annealing process, the hairpin solutions were combined, and 0.1-2.0 equiv. of initiator strands were immediately added to the mixture. The reaction was gently shaken overnight at room temperature. The nanostructures were then purified by aqueous GPC and dialyzed into PBS for further experiments.

Synthesis of PEG-DNA conjugates

PEGylation of the hairpins was achieved *via* click reaction between DBCO-modified DNA and azide-terminated PEG. In a typical reaction, azide-functionalized 10 kDa PEG (150 nmol) and DBCO-modified hairpin strands (100 nmol) were dissolved in 3 M sodium chloride solution in a microcentrifuge tube. The mixture was shaken gently overnight at 50 °C on an Eppendorf Thermomixer C. Unreacted PEG and DNA were removed by reversed-phase HPLC. The final solution was lyophilized to yield powdery solids. All DNA and PEGylated DNA sequences were

characterized by agarose gel electrophoresis to confirm their structure and purity, and their concentration determined by UV-vis spectroscopy at 260 nm.

Pharmacological inhibition of cell uptake

Cells were seeded in 24-well plates at 2.0×10^5 cells per well in 1 mL complete RPMI culture medium and cultured for 24 h at 37 °C with 5% CO_2. Cells were then pretreated with 200 μL of RMPI that contains different inhibitors (10 mM NaN_3, 1 μg/mL chlorpromazine, 0.5 μg/mL filipin III, and 10 μg/mL fucoidan) for 30 min. Next, 200 μL of Cy3-labeled PEGylated hairpin and PEGylated DNA assemblies (10 μM ASO) were mixed with the corresponding inhibitor and added to cells. After 24 h, cells were washed with PBS 3× and suspended by treatment with trypsin. 2 mL of PBS was added to each culture well, and the solutions were centrifugated for 5 min (1000 rpm). Cells were then resuspended in 0.5 mL of PBS for flow cytometry analysis on a Invitrogen Attune NxT Flow Cytometer. Data for 1.0×10^4 gated events were collected.

Western blot

Cells were plated at a density of 2.0×10^5 cells per well in 24-well plates in RPMI medium and cultured overnight at 37°C with 5% CO_2. Thereafter, samples and controls (100 nM-10 μM equivalent of antisense DNA) in serum-free medium were added to the wells and cells were incubated for 6 hours, before fresh medium was used to replace the incubation mixture. Cells were cultured for another 66 hours before protein levels were measured. Cells were harvested following incubation, and whole-cell lysates were collected in 100 μl of radioimmunoprecipitation assay cell lysis buffer with 1 mM phenylmethylsulfonyl fluoride (Cell Signaling Technology Inc., MA, USA) following the manufacturer's protocol. Protein content in the extracts was quantified using a bicinchoninic acid protein assay kit (Thermo Fisher

Scientific, MA, USA). Equal amounts of proteins (30 μg per lane) were separated on 4 to 20% gradient SDS-polyacrylamide gel electrophoresis and electro-transferred to nitrocellulose membrane. The membranes were then blocked with 3% bovine serum albumin in tris-buffered saline supplemented with 0.05% Tween 20 and then probed with appropriate primary antibodies overnight at 4°C. After washing and incubation with secondary antibodies, detected protein bands were visualized by chemiluminescence using the ECL Western Blotting Substrate (Thermo Fisher Scientific, MA, USA). Antibodies used for Western blots were: KRAS antibody (cat. NBP2-45536; Novus Biologicals); vinculin clone hVIN-1 (cat. V9131; Sigma). anti-rabbit IgG, HRP-linked antibody (cat. 7074P2), anti-mouse IgG, HRP-linked antibody (cat. 7076S) were from Cell Signaling Technologies.

Plasma pharmacokinetics

Immunocompetent mice (C57BL/6) were used to examine the pharmacokinetics of hairpin, PEGylated hairpins, and DNA assemblies (with or without PEGylation). Mice were randomly divided into four groups (n = 4). Samples were intravenously administered via the tail vein at equal DNA concentrations (500 nmol/kg). Blood samples (50 μl) were collected from the submandibular vein at varying time points (30 min and 2, 4, and 8 hours) using BD Vacutainer blood collection tubes with sodium heparin. Heparinized plasma was obtained by centrifugation at 3000 rpm for 15 min, aliquoted into a 96-well plate, and measured for fluorescence intensity on BioTek Synergy HT (BioTek Instruments Inc., VT, USA). The amounts of DNA in the blood samples were estimated using standard curves established for each sample in freshly collected plasma. To establish the standard curves, samples of known quantities were incubated with freshly collected plasma for 1 hour at room temperature before fluorescence was measured.

Statistics

Statistical significance was evaluated by using two-tailed t test when only two groups were compared. If more than two groups were compared, evaluation of significance was performed using one-way analysis of variance (ANOVA) followed by Bonferroni's post hoc test. Statistical significance was set at $P < 0.01$ or $P < 0.001$.

ASSOCIATED CONTENT

Supporting Information.

The Supporting Information is available free of charge on the at DOI:

Additional instrumental and experimental details; table of DNA oligonucleotides; schematics of PEG-hairpin conjugation and hybridization chain reaction; agarose gel analysis of short-stem DNA assemblies; reversed-phase HPLC and aqueous GPC chromatograms of DNA assembly and monomers; DLS and zeta potential measurement of DNA assembly and monomers; additional TEM images; agarose gel analysis of the stability of DNA assembly and monomers in RPMI media, in the presence of DNase I and after lyophilization; cellular uptake of DNA assembly and monomers in PC9 cell lines; additional confocal microscopy images pharmacological inhibition study; relative expression of KRAS in NCI-H358 and PC9 cell lines.

AUTHOR INFORMATION

Corresponding Author

Ke Zhang - *Department of Chemistry and Chemical Biology, Northeastern University, Boston, Massachusetts 02115, United States;* ORCID 0000-0002-8142-6702

E-mail: k.zhang@northeastern.edu

Authors

Yuyan Wang - *Department of Chemistry and Chemical Biology, Northeastern University, Boston, Massachusetts 02115, United States*

Dali Wang - *Department of Chemistry and Chemical Biology, Northeastern University, Boston, Massachusetts 02115, United States*

Fei Jia - *Department of Chemistry and Chemical Biology, Northeastern University, Boston, Massachusetts 02115, United States*

Andrew Miller - *Department of Chemistry and Chemical Biology, Northeastern University, Boston, Massachusetts 02115, United States*

Xuyu Tan - *Department of Chemistry and Chemical Biology, Northeastern University, Boston, Massachusetts 02115, United States*

Peiru Chen - *Department of Chemistry and Chemical Biology, Northeastern University, Boston, Massachusetts 02115, United States*

Lei Zhang - *Department of Chemistry and Chemical Biology, Northeastern University, Boston, Massachusetts 02115, United States*

Hao Lu - *Department of Chemistry and Chemical Biology, Northeastern University, Boston, Massachusetts 02115, United States*

Yang Fang - *Department of Chemistry and Chemical Biology, Northeastern University, Boston, Massachusetts 02115, United States*

Xi Kang - *Department of Chemistry and Chemical Biology, Northeastern University, Boston, Massachusetts 02115, United States*

Jiansong Cai - *Department of Chemistry and Chemical Biology, Northeastern University, Boston, Massachusetts 02115, United States*

Mengqi Ren - *Department of Chemistry and Chemical Biology, Northeastern University, Boston, Massachusetts 02115, United States*

Author Contributions

K.Z. and Y.W. devised the experiments and wrote the manuscript. Y.W. conducted the synthesis of materials, purification and material/biological characterization. All other authors contributed to material synthesis, purification, and/or discussion of the results. All authors edited the manuscript.

Funding Sources

Research reported in this publication was supported by the National Institutes of Health (the National Institute of General Medical Sciences award number 1R01GM121612 and the National Cancer Institute award number 1R01CA251730) and the National Science Foundation (DMR award number 2004947).

Notes

The authors declare no competing financial interest.

ACKNOWLEDGMENT

The authors thank William Fowle at the NEU Biology Department for his expertise with the TEM, Dr. Heather Clark and Dr. Guoxin Rong for help with the confocal microscopy, and Dr. Jiahe Li as well as the Center for Pharmaceutical Biotechnology and Nanomedicine at Northeastern University for assistance with flow cytometry.

REFERENCES

1. Zamecnik, P. C.; Stephenson, M. L., Inhibition of Rous Sarcoma Virus Replication and Cell Transformation by a Specific Oligodeoxynucleotide. *P Natl Acad Sci Usa* **1978,** *75* (1), 280-284.
2. Rayburn, E. R.; Zhang, R., Antisense, Rnai, and Gene Silencing Strategies for Therapy: Mission Possible or Impossible? *Drug Discov Today* **2008,** *13* (11-12), 513-521.
3. Hyde, S. C.; Gill, D. R.; Higgins, C. F.; Trezise, A. E. O.; MacVinish, L. J.; Cuthbert, A. W.; Ratcliff, R.; Evans, M. J.; Colledge, W. H., Correction of the Ion Transport Defect in Cystic Fibrosis Transgenic Mice by Gene Therapy. *Nature* **1993,** *362* (6417), 250-255.
4. Aartsma-Rus, A.; Corey, D. R., The 10th Oligonucleotide Therapy Approved: Golodirsen for Duchenne Muscular Dystrophy. *Nucleic Acid Ther* **2020,** *30* (2), 67-70.
5. Abdelhady, H. G.; Allen, S.; Davies, M. C.; Roberts, C. J.; Tendler, S. J. B.; Williams, P. M., Direct Real-Time Molecular Scale Visualisation of the Degradation of Condensed DNA Complexes Exposed to Dnase I. *Nucleic Acids Res* **2003,** *31* (14), 4001-4005.
6. Medzhitov, R., Toll-Like Receptors and Innate Immunity. *Nat Rev Immunol* **2001,** *1* (2), 135-145.
7. Hoke, G. D.; Draper, K.; Freier, S. M.; Gonzalez, C.; Driver, V. B.; Zounes, M. C.; Ecker, D. J., Effects of Phosphorothioate Capping on Antisense Oligonucleotide Stability, Hybridization and Antiviral Efficacy Versus Herpes Simplex Virus Infection. *Nucleic Acids Res* **1991,** *19* (20), 5743-5748.
8. Deleavey, Glen F.; Damha, Masad J., Designing Chemically Modified Oligonucleotides for Targeted Gene Silencing. *Chem Biol* **2012,** *19* (8), 937-954.
9. Cho-Chung, Y. S., Antisense Dnas as Targeted Genetic Medicine to Treat Cancer. *Arch Pharm Res* **2003,** *26* (3), 183-191.
10. Juliano, R. L., The Delivery of Therapeutic Oligonucleotides. *Nucleic Acids Res* **2016,** *44* (14), 6518-6548.
11. Bae, W.; Kocabey, S.; Liedl, T., DNA Nanostructures in Vitro, in Vivo and on Membranes. *Nano Today* **2019,** *26*, 98-107.
12. Li, J.; Pei, H.; Zhu, B.; Liang, L.; Wei, M.; He, Y.; Chen, N.; Li, D.; Huang, Q.; Fan, C., Self-Assembled Multivalent DNA Nanostructures for Noninvasive Intracellular Delivery of Immunostimulatory Cpg Oligonucleotides. *Acs Nano* **2011,** *5* (11), 8783-8789.
13. Ponnuswamy, N.; Bastings, M. M. C.; Nathwani, B.; Ryu, J. H.; Chou, L. Y. T.; Vinther, M.; Li, W. A.; Anastassacos, F. M.; Mooney, D. J.; Shih, W. M., Oligolysine-Based Coating Protects DNA Nanostructures from Low-Salt Denaturation and Nuclease Degradation. *Nat. Commum.* **2017,** *8* (1), 15654.

14. Zhang, Y.; Lu, F.; Yager, K. G.; van der Lelie, D.; Gang, O., A General Strategy for the DNA-Mediated Self-Assembly of Functional Nanoparticles into Heterogeneous Systems. *Nat. Nanotechnol.* **2013,** *8* (11), 865-872.
15. Lv, H.; Zhang, S.; Wang, B.; Cui, S.; Yan, J., Toxicity of Cationic Lipids and Cationic Polymers in Gene Delivery. *J Control Release* **2006,** *114* (1), 100-109.
16. Andrew, D. M., The Problem with Cationic Liposome / Micelle-Based Non-Viral Vector Systems for Gene Therapy. *Curr Med Chem* **2003,** *10* (14), 1195-1211.
17. Chakraborty, C.; Sharma, A. R.; Sharma, G.; Doss, C. G. P.; Lee, S.-S., Therapeutic Mirna and Sirna: Moving from Bench to Clinic as Next Generation Medicine. *Mol Ther Nucleic Acids* **2017,** *8*, 132-143.
18. Harris, J. M.; Chess, R. B., Effect of Pegylation on Pharmaceuticals. *Nat Rev Drug Discov* **2003,** *2* (3), 214-221.
19. Lu, X.; Zhang, K., Pegylation of Therapeutic Oligonucletides: From Linear to Highly Branched Peg Architectures. *Nano Research* **2018,** *11* (10), 5519-5534.
20. Ng, E. W. M.; Shima, D. T.; Calias, P.; Cunningham, E. T.; Guyer, D. R.; Adamis, A. P., Pegaptanib, a Targeted Anti-Vegf Aptamer for Ocular Vascular Disease. *Nat Rev Drug Discov* **2006,** *5* (2), 123-132.
21. Winkler, J., Therapeutic Oligonucleotides with Polyethylene Glycol Modifications. *Future Med Chem* **2015,** *7* (13), 1721-1731.
22. Jia, F.; Lu, X.; Wang, D.; Cao, X.; Tan, X.; Lu, H.; Zhang, K., Depth-Profiling the Nuclease Stability and the Gene Silencing Efficacy of Brush-Architectured Poly(Ethylene Glycol)–DNA Conjugates. *J Am Chem Soc* **2017,** *139* (31), 10605-10608.
23. Lu, X.; Jia, F.; Tan, X.; Wang, D.; Cao, X.; Zheng, J.; Zhang, K., Effective Antisense Gene Regulation Via Noncationic, Polyethylene Glycol Brushes. *J Am Chem Soc* **2016,** *138* (29), 9097-9100.
24. Li, H.; Li, Y.; Xiao, Y.; Zhang, B.; Cheng, Z.; Shi, J.; Xiong, J.; Li, Z.; Zhang, K., Well-Defined DNA–Polymer Miktoarm Stars for Enzyme-Resistant Nanoflares and Carrier-Free Gene Regulation. *Bioconjugate Chem* **2020,** *31* (3), 530-536.
25. Jia, F.; Lu, X.; Tan, X.; Wang, D.; Cao, X.; Zhang, K., Effect of Peg Architecture on the Hybridization Thermodynamics and Protein Accessibility of Pegylated Oligonucleotides. *Angew. Chem. Int. Ed.* **2017,** *56* (5), 1239-1243.
26. Wang, D.; Lin, J.; Jia, F.; Tan, X.; Wang, Y.; Sun, X.; Cao, X.; Che, F.; Lu, H.; Gao, X.; Shimkonis, J. C.; Nyoni, Z.; Lu, X.; Zhang, K., Bottlebrush-Architectured Poly(Ethylene Glycol) as an Efficient Vector for Rna Interference in Vivo. *Sci. Adv.* **2019,** *5* (2), eaav9322.
27. Jia, F.; Wang, D.; Lu, X.; Tan, X.; Wang, Y.; Lu, H.; Zhang, K., Improving the Enzymatic Stability and the Pharmacokinetics of Oligonucleotides Via DNA-Backboned Bottlebrush Polymers. *Nano Lett* **2018,** *18* (11), 7378-7382.
28. Liu, J.; Lu, Y., A Colorimetric Lead Biosensor Using Dnazyme-Directed Assembly of Gold Nanoparticles. *J Am Chem Soc* **2003,** *125* (22), 6642-6643.
29. Jia, H.; Shi, J.; Ren, W.; Zhao, J.; Dong, Y.; Liu, D., Controllable Supramolecular "Ring Opening" Polymerization Based on DNA Duplex. *Polymer* **2019,** *171*, 121-126.
30. Dirks, R. M.; Pierce, N. A., Triggered Amplification by Hybridization Chain Reaction. *P Natl Acad Sci Usa* **2004,** *101* (43), 15275.
31. Yang, B.; Zhang, X.-B.; Kang, L.-P.; Shen, G.-L.; Yu, R.-Q.; Tan, W., Target-Triggered Cyclic Assembly of DNA–Protein Hybrid Nanowires for Dual-Amplified Fluorescence Anisotropy Assay of Small Molecules. *Anal Chem* **2013,** *85* (23), 11518-11523.

32. Chang, X.; Zhang, C.; Lv, C.; Sun, Y.; Zhang, M.; Zhao, Y.; Yang, L.; Han, D.; Tan, W., Construction of a Multiple-Aptamer-Based DNA Logic Device on Live Cell Membranes Via Associative Toehold Activation for Accurate Cancer Cell Identification. *J Am Chem Soc* **2019,** *141* (32), 12738-12743.
33. Seeman, N. C.; Sleiman, H. F., DNA Nanotechnology. *Nature Reviews Materials* **2017,** *3* (1), 17068.
34. Ross, S. J.; Revenko, A. S.; Hanson, L. L.; Ellston, R.; Staniszewska, A.; Whalley, N.; Pandey, S. K.; Revill, M.; Rooney, C.; Buckett, L. K.; Klein, S. K.; Hudson, K.; Monia, B. P.; Zinda, M.; Blakey, D. C.; Lyne, P. D.; Macleod, A. R., Targeting Kras-Dependent Tumors with Azd4785, a High-Affinity Therapeutic Antisense Oligonucleotide Inhibitor of Kras. *Sci Transl Med* **2017,** *9* (394).
35. O'Reilly, R. K.; Joralemon, M. J.; Wooley, K. L.; Hawker, C. J., Functionalization of Micelles and Shell Cross-Linked Nanoparticles Using Click Chemistry. *Chem Mater* **2005,** *17* (24), 5976-5988.
36. Li, H.; Zhang, B.; Lu, X.; Tan, X.; Jia, F.; Xiao, Y.; Cheng, Z.; Li, Y.; Silva, D. O.; Schrekker, H. S.; Zhang, K.; Mirkin, C. A., Molecular Spherical Nucleic Acids. *P Natl Acad Sci Usa* **2018,** *115* (17), 4340-4344.
37. Keum, J.-W.; Bermudez, H., Enhanced Resistance of Dnananostructures to Enzymatic Digestion. *Chem Commun* **2009,** (45), 7036-7038.
38. Lacroix, A.; Vengut-Climent, E.; de Rochambeau, D.; Sleiman, H. F., Uptake and Fate of Fluorescently Labeled DNA Nanostructures in Cellular Environments: A Cautionary Tale. *ACS Central Science* **2019,** *5* (5), 882-891.
39. Choi, C. H. J.; Hao, L.; Narayan, S. P.; Auyeung, E.; Mirkin, C. A., Mechanism for the Endocytosis of Spherical Nucleic Acid Nanoparticle Conjugates. *Proceedings of the National Academy of Sciences* **2013,** *110* (19), 7625.
40. Koller, E.; Vincent, T. M.; Chappell, A.; De, S.; Manoharan, M.; Bennett, C. F., Mechanisms of Single-Stranded Phosphorothioate Modified Antisense Oligonucleotide Accumulation in Hepatocytes. *Nucleic Acids Res* **2011,** *39* (11), 4795-4807.
41. Crooke, S. T.; Wang, S.; Vickers, T. A.; Shen, W.; Liang, X.-h., Cellular Uptake and Trafficking of Antisense Oligonucleotides. *Nat Biotechnol* **2017,** *35* (3), 230-237.

Scheme 1. Preparation of DNA bottlebrushes with PEG side chains by hybridization chain reaction.

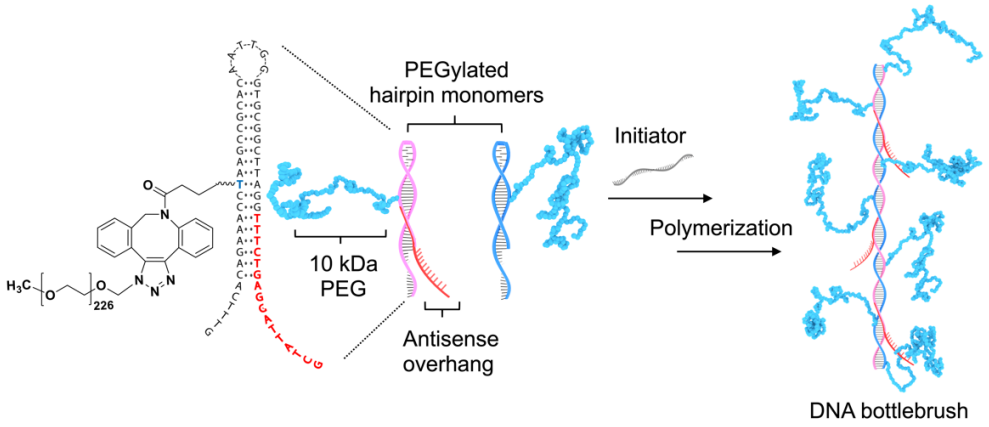

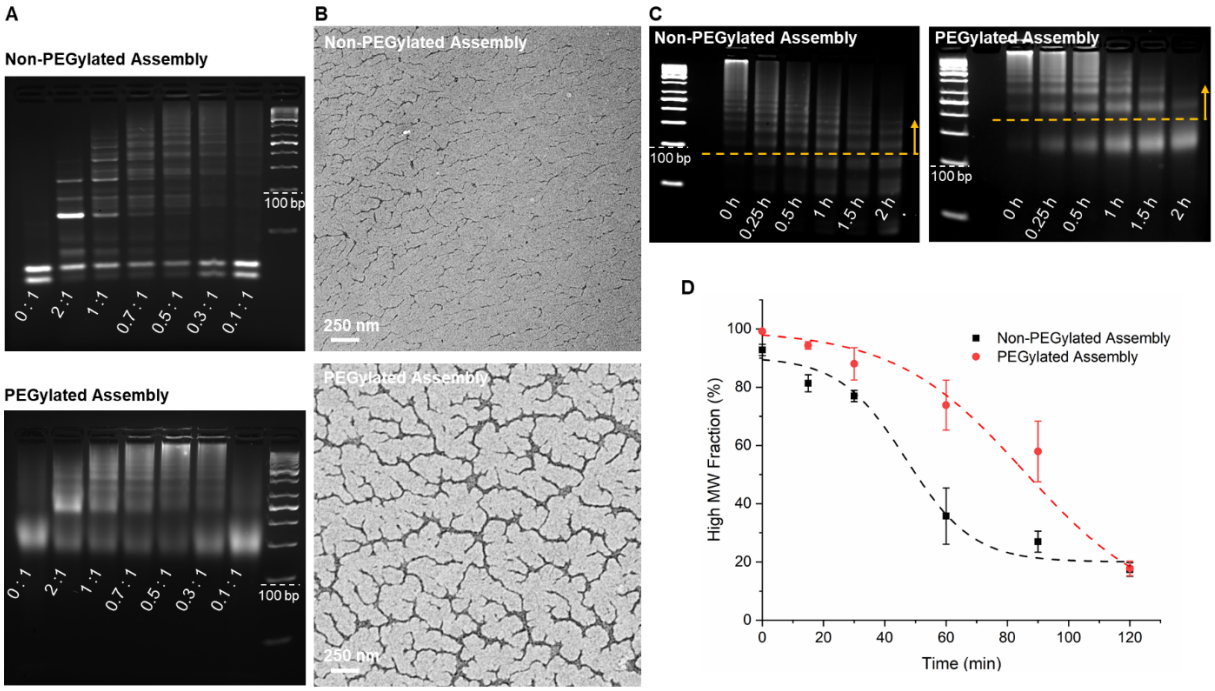

Figure. 1. A) Agarose gel (5%) electrophoresis analysis of DNA assemblies as a function of initiator:hairpin ratio. **B**) TEM images (negatively stained with 2% uranyl acetate) of DNA assemblies with or without PEGylation. **C**) Agarose gel electrophoresis of DNA assembly samples treated with DNase I for various amounts of time (EB channel). Dashed line indicates a cut-off for high molecular weight fractions (>50 kDa). **D**) High molecular weight fractions as a function of DNase I treatment time.

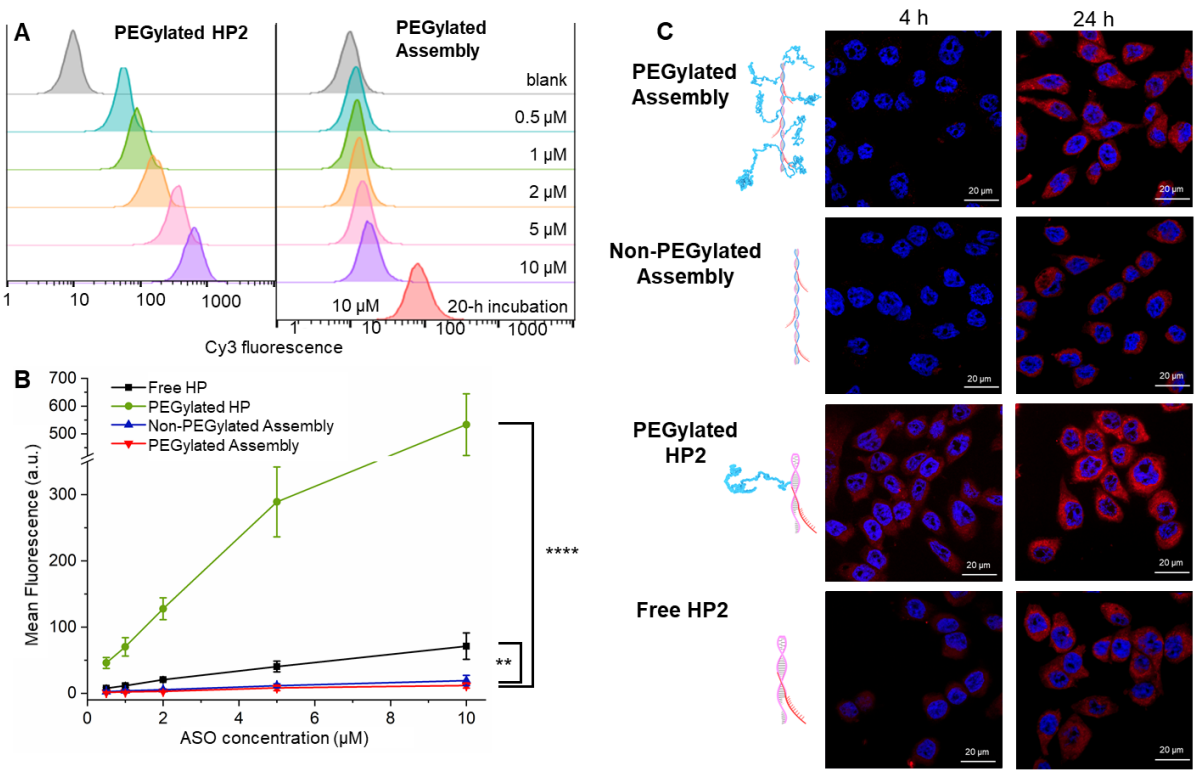

Figure 2. A) Flow cytometry measurement of NCI-H358 cells treated with Cy3-labeled PEG-hairpins and assemblies ([monomer]: 0.5 to 10 μM) for 4 hours. **B)** Mean fluorescence intensity of cells treated with Cy3-labeled DNA assemblies and their precursors. **C)** Confocal microscopy images of cells treated with Cy5-labeled DNA assemblies and their precursors for 4 and 24 h. ***P*<0.01, *****P*<0.0001 (two-tailed test).

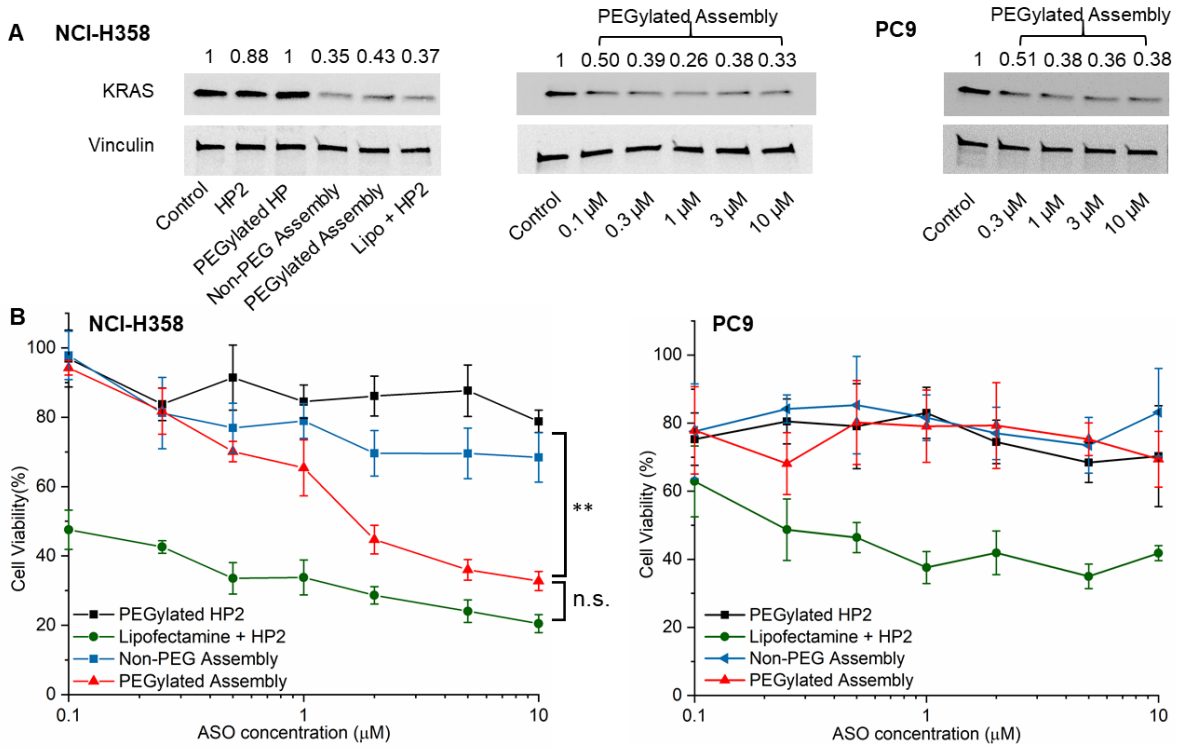

Figure 3. A) Western blot analysis of cell lysates from NCI-H358 or PC9 cells after treatment for 72 hours with DNA assemblies and controls. **B)** Cell viability of NCI-H358 and PC9 cells treated with assemblies and controls as determined by an MTT assay. $^{**}P<0.01$ (two-tailed *t* test).

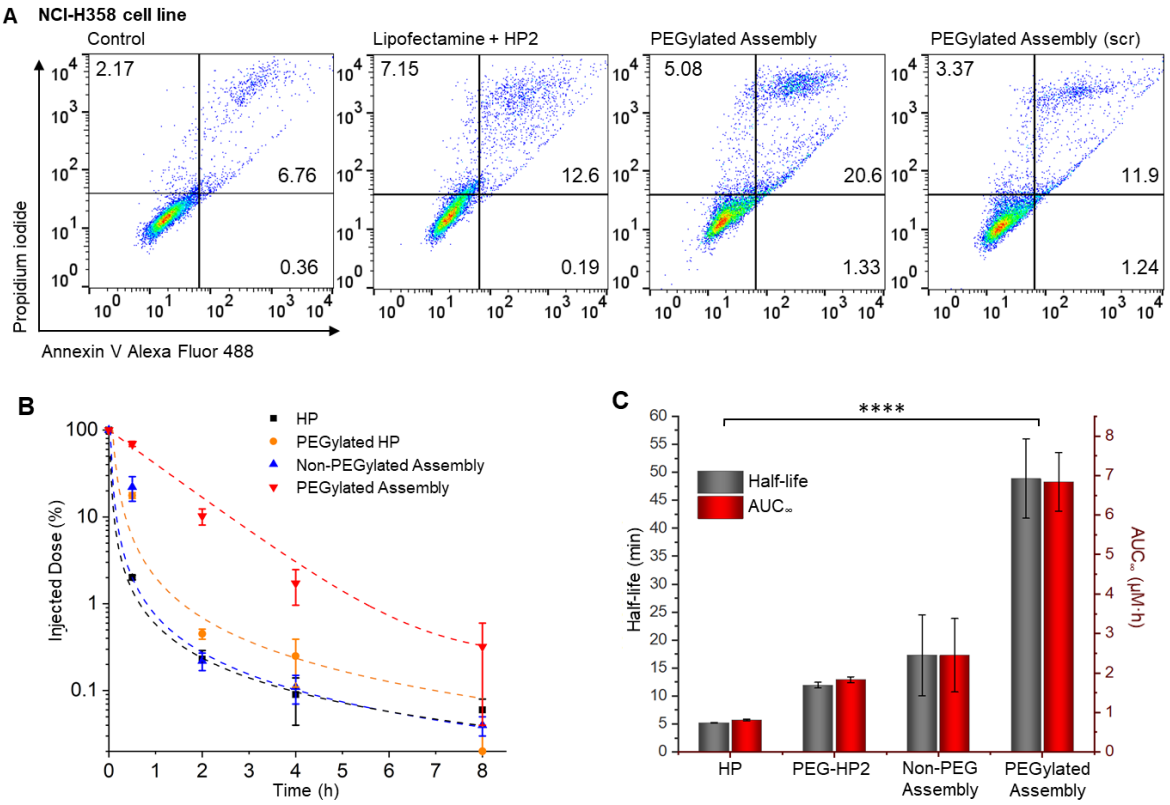

Figure 4. (A) Cell apoptosis following sample treatment determined by staining with annexin V and propidium iodide (PI). Early apoptotic, late apoptotic, and necrotic cell populations (%) are shown in the lower right, upper right, and upper left quadrants, respectively. **B)** Plasma pharmacokinetics of hairpins and DNA assemblies (with or without PEGylation) in C57BL/6 mice. **C)** Plasma half-life and blood availability of DNA assemblies and their precursors. ****P<0.0001 (ANOVA)

TOC

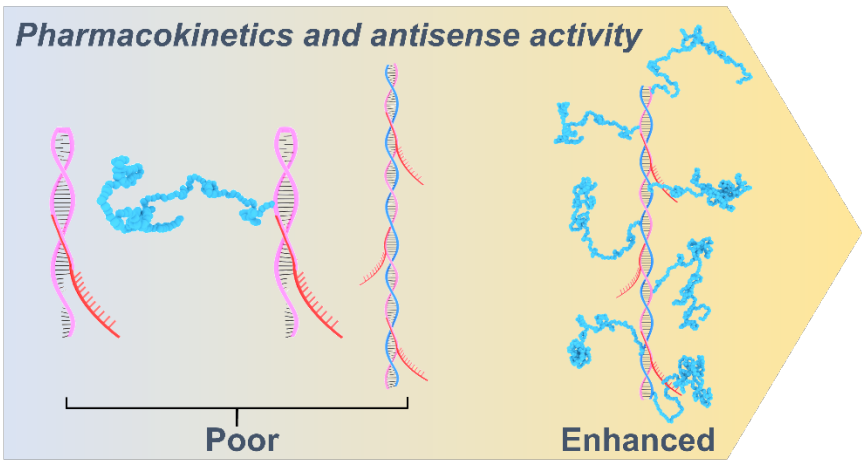

Supporting Information for

Self-Assembled DNA-PEG Bottlebrushes Enhance Antisense Activity and Pharmacokinetics of Oligonucleotides

*Yuyan Wang, Dali Wang, Fei Jia, Andrew Miller, Xuyu Tan, Peiru Chen, Lei Zhang, Hao Lu, Yang Fang, Xi Kang, Jiansong Cai, Mengqi Ren, and Ke Zhang**

Department of Chemistry and Chemical Biology, Northeastern University Boston
Massachusetts 02115, United States
To whom correspondence should be addressed.
E-mail: k.zhang@northeastern.edu

Materials and methods

Phosphoramidites and supplies for DNA synthesis were purchased from Glen Research Co (Sterling, VA, USA). Azide-terminated poly(ethylene glycol) methyl ether (M_n = 10 kDa, PDI<1.05) was purchased from Sigma-Aldrich Co (St. Louis, MO, USA). Human NCI-H358 cell lines were purchased from American Type Culture Collection (Rockville, MD, USA). Human PC9 cell lines were from Dr. Zhao's lab (Dana-Farber Cancer Institute). All other materials were purchased from Fisher Scientific Inc. (Waltham, MA, USA), Sigma-Aldrich Co., and VWR International LLC. (Franklin, MA, USA), and used as received unless otherwise indicated. Aqueous GPC measurements were performed on a Waters Breeze 2 GPC system equipped with Ultrahydrogel™ 500 and Ultrahydrogel™ 250, 7.8Å×300 mm column and a 2998 PDA detector (Waters Co., MA, USA). Phosphate-buffered saline (PBS, pH 7.4) was used as the eluent running at a flow rate of 0.8 mL/min. Reversed-phase HPLC was performed using a Waters Breeze 2 HPLC system coupled to a Symmetry C18 3.5 μm, 4.6Å×75 mm reversed-phase column and a 2998 PDA detector. Gel electrophoresis was performed using 5% agarose gel in 0.5× tris/borate/EDTA (TBE) buffer with a running voltage of 120 V. Gel images were acquired on an Alpha Innotech Fluorochem Q imager. All TEM samples were imaged on a JEOL JEM 1010 electron microscope utilizing an accelerating voltage of 80 kV. DLS and ζ potential data were recorded on a Malvern Zetasizer Nano-ZSP (Malvern, UK).

Oligonucleotide synthesis

Oligonucleotides were synthesized on an ABI Model 391 DNA synthesizer (Applied Biosystems, Inc., Foster City, CA) using standard solid-phase phosphoramidite methodology. DNA strands were cleaved from the CPG support using aqueous ammonium hydroxide (28-30% NH_3 basis) at room temperature for 24 h. All DNA strands were then purified by reversed-phase HPLC. Mobile phases for HPLC purification are triethylammonium acetate (TEAA) buffer (0.1 M) and HPLC-grade acetonitrile, with a flow rate of 1 mL/min. The gradient method starts from 100% TEAA, increasing acetonitrile to 100% in 50 mins. The dimethoxytrityl protecting groups were subsequently removed by treatment with 20% acetic acid for 1 h, and extracted with ethyl acetate three times in an aqueous solution. Upon lyophilization, DNA was collected and stored at -20°C. To synthesize modified DNA strands, Cyanine 3 CPG and Cyanine 5 CPG were used as the solid support and DBCO-modified dT was used to install DBCO-functional group to the DNA strands.

Cell culture

NCI-H358 and PC9 cells were cultured in RPMI supplied with 10% fetal bovine serum (FBS), 1% L-glutamine, and 1% antibiotics at 37°C in a humidified atmosphere containing 5% CO_2.

Dynamic Light Scattering

1 mL of DLS sample at 10 μM was dialyzed into PBS buffer, and then filtered through a 0.2 μm PTFE filter. The sample solution was added into a disposable cuvette for measurement. Data was recorded under 173° backscatter measurement angle.

Transmission Electron Microscopy

1 μM of TEM samples was deposited on carbon-coated copper grids for 10 min before being carefully wicked away by filter paper. The grids were then stained by depositing on 10 μL of 1% uranyl acetate. The stain was allowed to stay for 3 min before being wicked away.

Nuclease degradation kinetics

1 μM of Cy5-labeled DNA assemblies (with or without PEGylation) were incubated with DNase I (0.4 unit/mL, Sigma-Aldrich) in PBS buffer solution (with 2.5 mM $MgCl_2$ and 0.5 mM $CaCl_2$) for 15 min, 30 min, 1h, 1.5h and 2h with gentle shaking on an Eppendorf Thermomixer C at 37°C. Thereafter, the reaction mixture was immediately mixed with loading buffer and transferred into a pre-cast 5% agarose gel. Then the gel was electrophoresed in 0.5× TBE buffer at a constant voltage of 120 V. The gel was then imaged and analyzed by an Alpha Innotech Fluorochem Q imager using band densitometry analysis.

Flow cytometry

Cells were seeded in 24-well plates at 2.0×10^5 cells per well in 1 mL complete RPMI and cultured for 24 h at 37°C with 5% CO_2. Then, Cy3-labeled hairpin strands, PEGylated hairpin strands, non-PEGylated assemblies, and PEGylated assemblies (500 nM-10 μM equiv. of antisense DNA) dissolved in serum-free RPMI culture medium were added, and cells were further incubated at 37°C for 4 h or 24 h. Subsequently, cells were washed with PBS 3× and suspended by treatment with trypsin. Thereafter, 2 mL of PBS was added to each culture well, and the solutions were centrifugated for 5 min (1000 rpm). Cells were then resuspended in 0.5 mL of PBS for flow cytometry analysis on a BD FACS Calibur flow cytometer. Data for 1.0×10^4 gated events were collected.

Serum stability test

1 nmol of Cy5-labeled unmodified hairpins, PEGylated hairpins, non-PEGylated assembly and PEGylated assembly were each dissolved in 100 μL full-serum RPMI media (10% FBS). 10 uL of each sample mixture was immediately taken out as the t = 0 h and stored at -20℃. The remaining samples were then incubated at 37℃, and 10 uL of each mixture sample was taken out at different time points: 1 h, 2 h, 4 h, 10 h and 24 h, and then stored at -20℃. Thereafter, the collected samples were analyzed by AGE (5%) and imaged under EB and Cy5 channel, separately.

Confocal microscopy

Cells were seeded in 24-well glass bottom plates at 1.0×10^5 cells per well and cultured in 1 mL complete RPMI for 24 h at 37°C with 5% CO_2. Then, Cy3- or Cy5-labeled hairpins, PEGylated hairpins, non-PEGylated assemblies, and PEGylated assemblies (10 μM equiv. of ASO) dissolved in serum-free RPMI media or complete RPMI culture medium were added and cells were incubated at 37°C for 4 h and 24 h. Thereafter, cells were washed with PBS 3× and fixed with 4% paraformaldehyde for 30 min at room temperature. After fixation, cells were washed with PBS 3× and kept in PBS. Then cells were stained with Hoechst 33342 for 10 min. The cells were imaged on an LSM-800 confocal laser scanning microscope (Carl Zeiss Ltd., Cambridge, UK). Imaging settings were kept identical for all samples.

MTT assay

The cytotoxicity of DNA assemblies and controls were evaluated with the MTT assay against NCI-H358 and PC9 cells. Briefly, cells were seeded into 96-well plates at 1.0×10^4 cells per well in 200 μL complete RMPI culture medium and cultured for 24 h. The cells were then treated with PEGylated hairpins, PEGylated DNA assemblies, and lipofectamine-complexed hairpins at varying concentrations (100 nM-10 μM equiv. of antisense DNA). Cells treated with vehicle (PBS) were used as a negative control, and Lipofectamine 2000 (Invitrogen Co., CA, USA)-treated cells

were used as a positive control. After 48 h of incubation, 20 μL of 5 mg/mL MTT stock solution in PBS was added to each well. The cells were incubated for another 4 h, and the medium containing unreacted MTT was removed carefully. The resulting blue formazan crystals were dissolved in 200 μL DMSO per well, and the absorbances (490 nm) were measured on a BioTek® Synergy™ Neo2 Multi-Mode microplate reader (BioTek Inc., VT, USA).

Cell apoptosis

NCI-H358 cells were treated with DNA assemblies and controls in the same fashion as those used in the Western blotting study. For the apoptosis analysis, both floating and attached cells were harvested, rinsed 3× with cold PBS, stained with Alexa Fluor 488 annexin V and PI, and analyzed by flow cytometry to identify apoptotic cells.

Table S1. All DNA sequences used in this study.[1-2]

System	Strand	Sequences*
Short-length	HP1	5'-**GCT ATT A** GGAGT CTT TAT AGT AAT CTCTA ATT ACT ATA AAG-3'
	HP2	5'-ATT ACT ATA AAG ACTCC CTT TAT AGT AAT TA*AG*-3'
	Initiator	5'-ATT ACT ATA AAG ACT CCT AAT AGC-3'
Long-length	HP1	5'-TTAACC CAC GCC GAA TCC AAA GAC CAAAGT GTC TTT GGA TTC GGC GTG-3'
	HP2	5'-**GCT ATT AGG A** GTC TTT GGA TTCGG CGT G GGTTAA CA CGC CGA ATC CAA AGA C ACTTTG-3'
	Initiator	5'-GTC TTT GGA TTC GGC GTG GGT TAA-3'
	Cy3-HP2	5'-**GCT ATT AGG A** GTC TTT GGA TTCGG CGT G GGTTAA CA CGC CGA ATC CAA AGA C ACTTTG-Cy3-3'
	Cy5-HP2	5'-**GCT ATT AGG A** GTC TTT GGA TTCGG CGT G GGTTAA CA CGC CGA ATC CAA AGA C ACTTTG-Cy5-3'
	SCR-HP2	5'-ACT GCG TTA GAG TAG GTA GAA GAT TAA CCA GTC TGG TTC GCT GCA GTC TCT GCT AGA C -3'
	Overhang-SCR-HP2	5'-**ATG TGA TCA G** GTC TTT GGA TTCGG CGT G GGTTAA CA CGC CGA ATC CAA AGA C ACTTTG-3'

*Modified T bases for PEGylation are marked in red. Hairpin loops are underlined and sticky ends are overlined. Overhangs are bolded. Antisense region is marked in blue.

Scheme S1. Assembly of bottlebrush-like nanostructures via hybridization chain reaction.

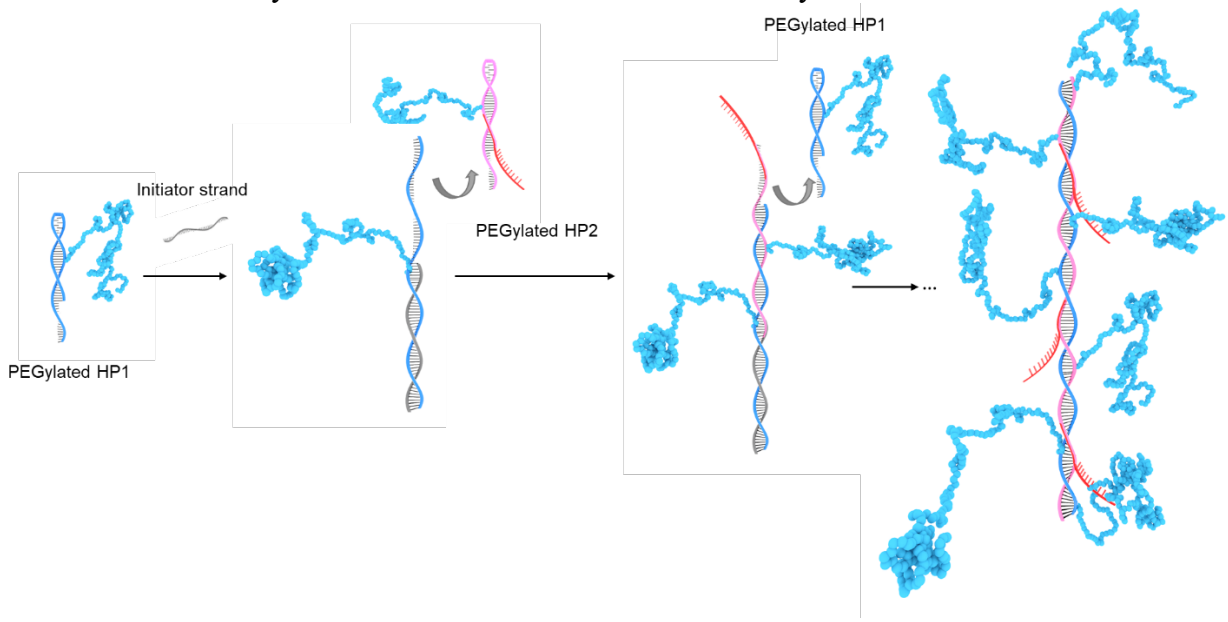

Scheme S2. Conjugation of azide-terminated PEG to DBCO-modified T base.

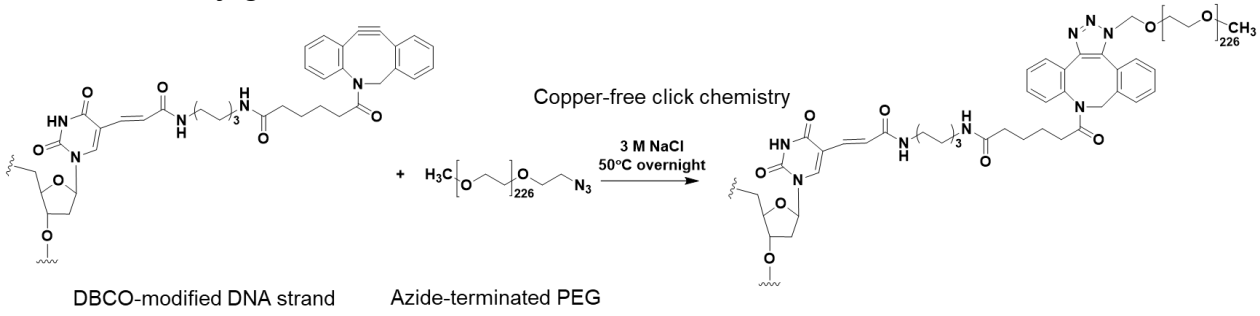

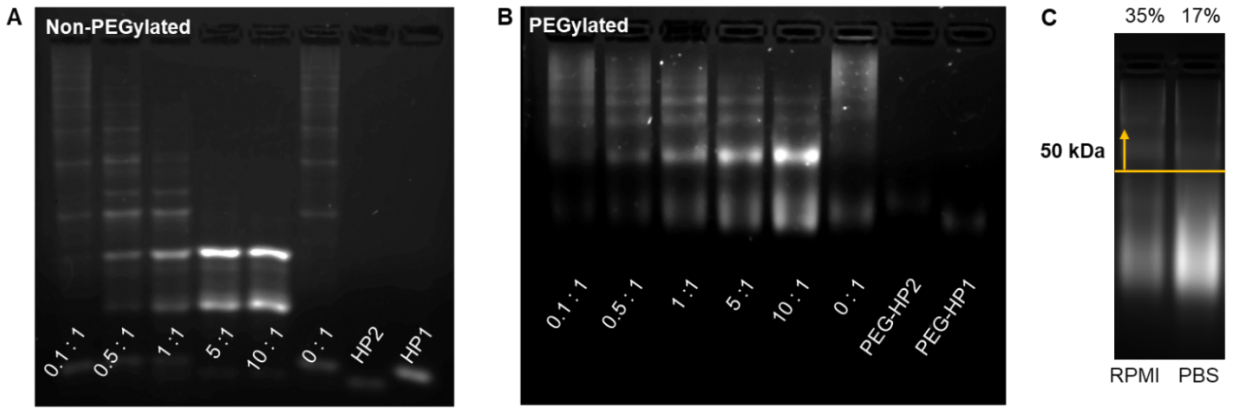

Fig. S1. A, B) AGE (5%) analysis of short-stem DNA assemblies as a function of initiator:hairpin ratio. **C)** AGE (5%) analysis of short-stem PEGylated DNA assemblies after dialysis into RPMI medium or PBS.

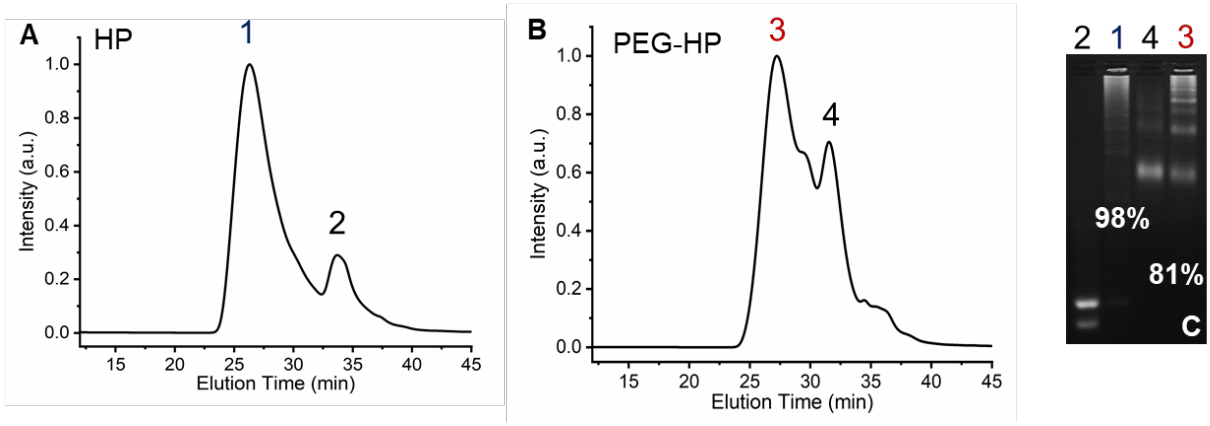

Fig. S2. A, B) Aqueous GPC purification of DNA assemblies. **C)** AGE (5%) analysis of high MW fraction of DNA assemblies after purification. Purity is determined by gel band densitometry analysis. 1-4: non-PEGylated assemblies, hairpin monomers, PEGylated assemblies, and PEGylated hairpin monomers, respectively.

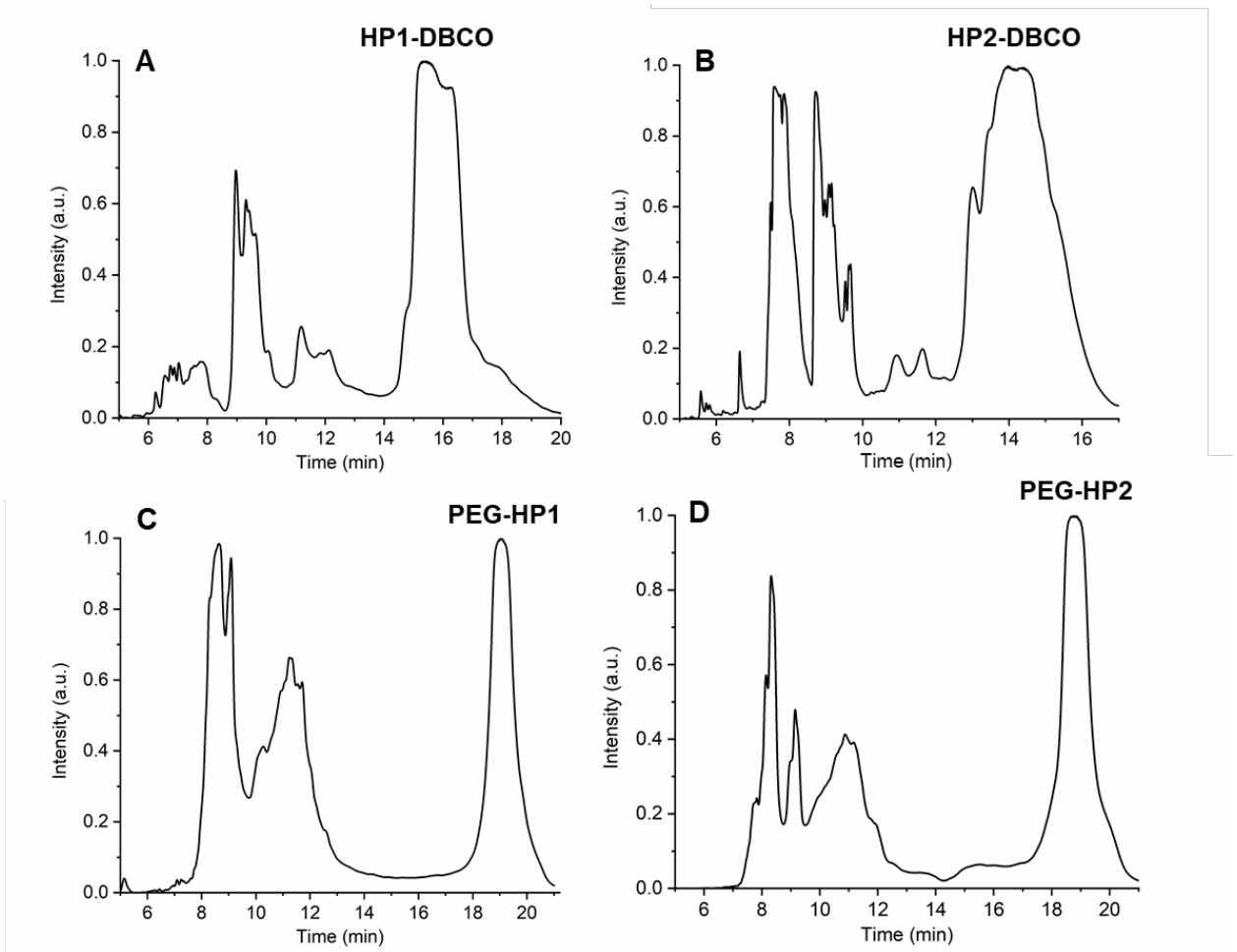

Fig. S3. A, B) Reversed-phase HPLC purification of DBCO-modified hairpin strands. **C, D)** Reversed-phase HPLC purification of PEGylated hairpin monomers.

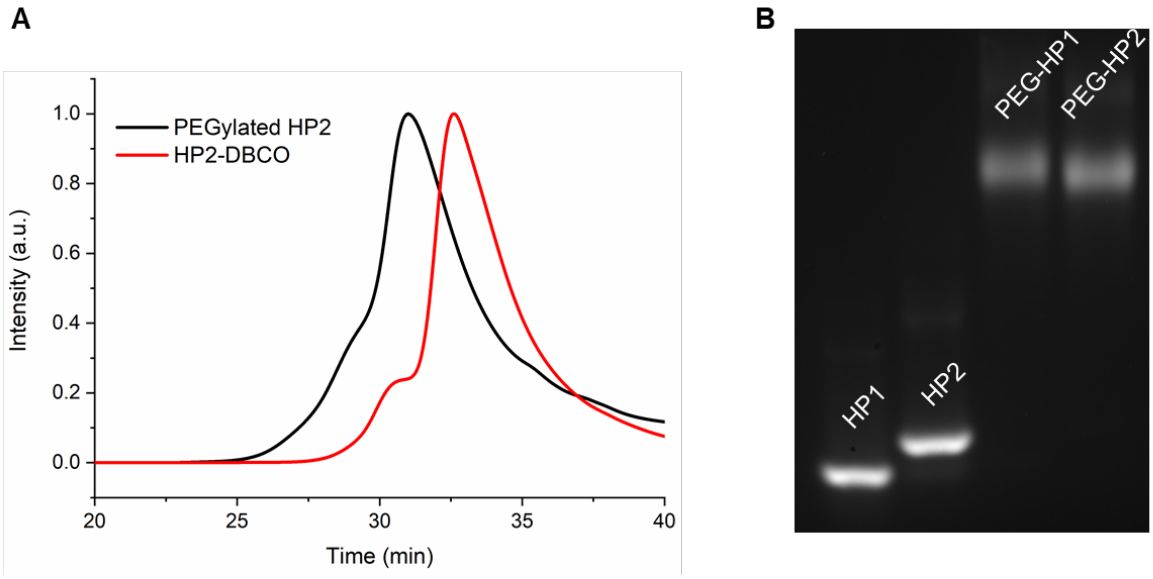

Fig. S4. A) Aqueous GPC chromatogram of DBCO-modified hairpin and PEGylated hairpins. **B)** AGE (2%) analysis of hairpins and PEGylated hairpins.

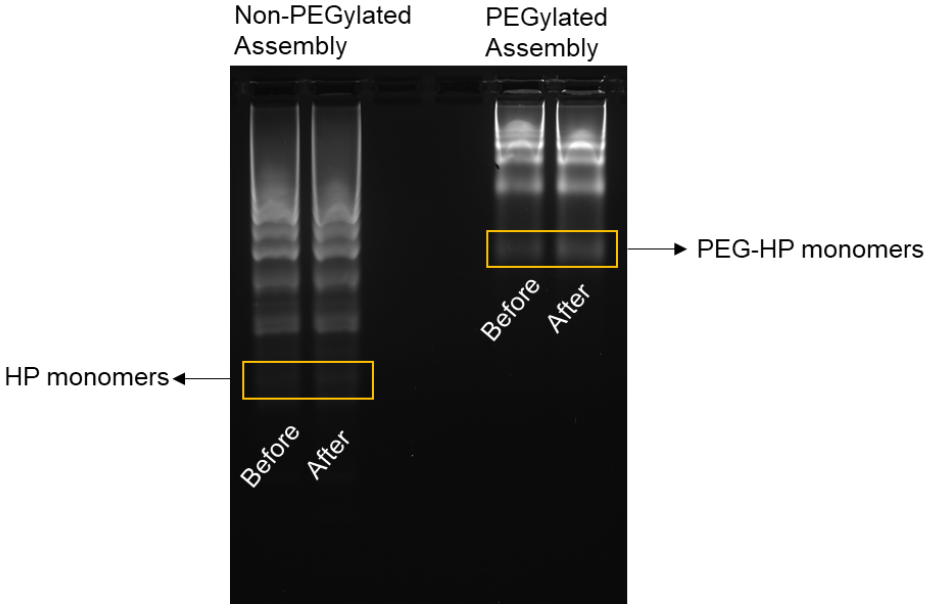

Fig. S5. AGE (5%) analysis of DNA assemblies before and after lyophilization.

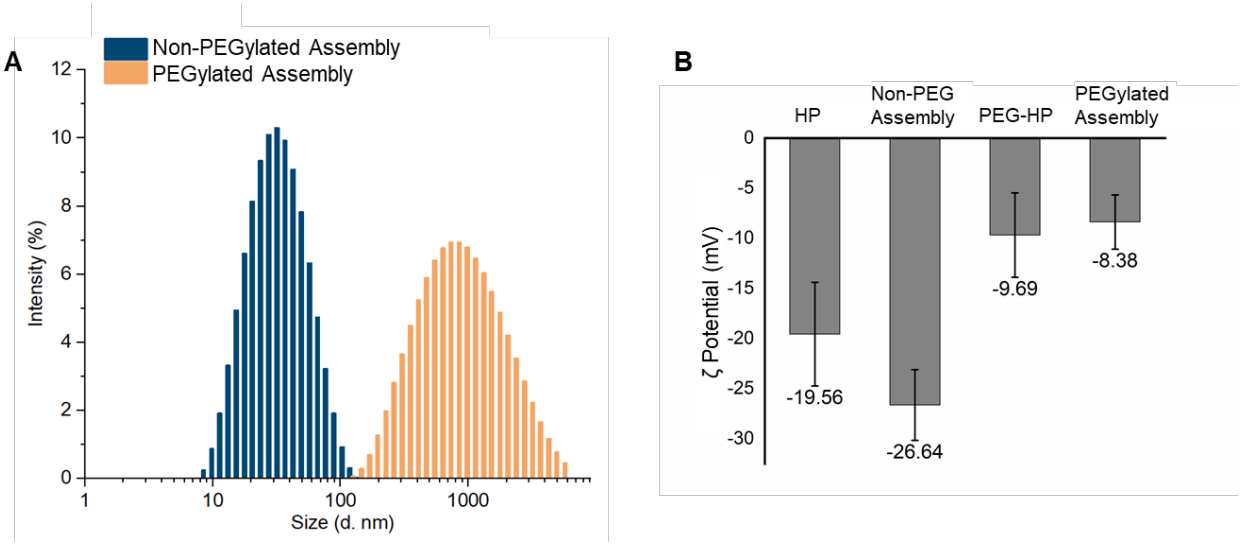

Fig. S6. A) DLS intensity-average hydrodynamic diameter distribution of DNA assemblies (with or without PEGylation). **(B)** ζ potential measurement of DNA assemblies and their precursors in PBS.

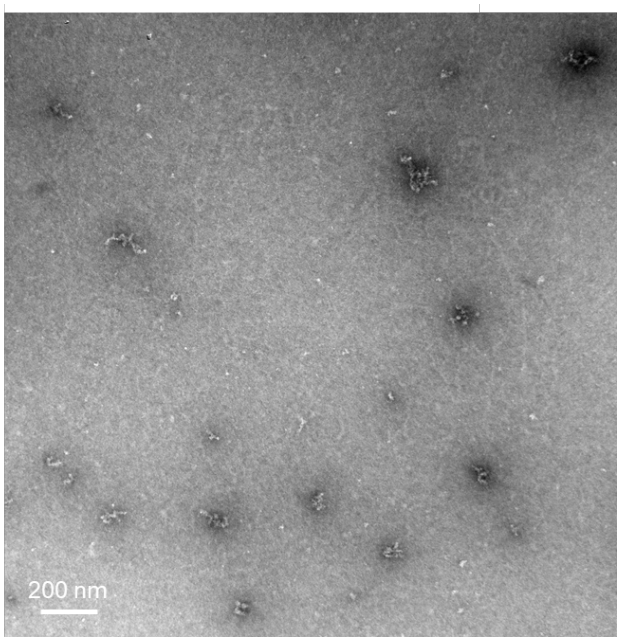

Fig. S7. TEM image (negatively stained with 2% uranyl acetate) of a physical mixture of DBCO-modified HP2 and 10 kDa PEG.

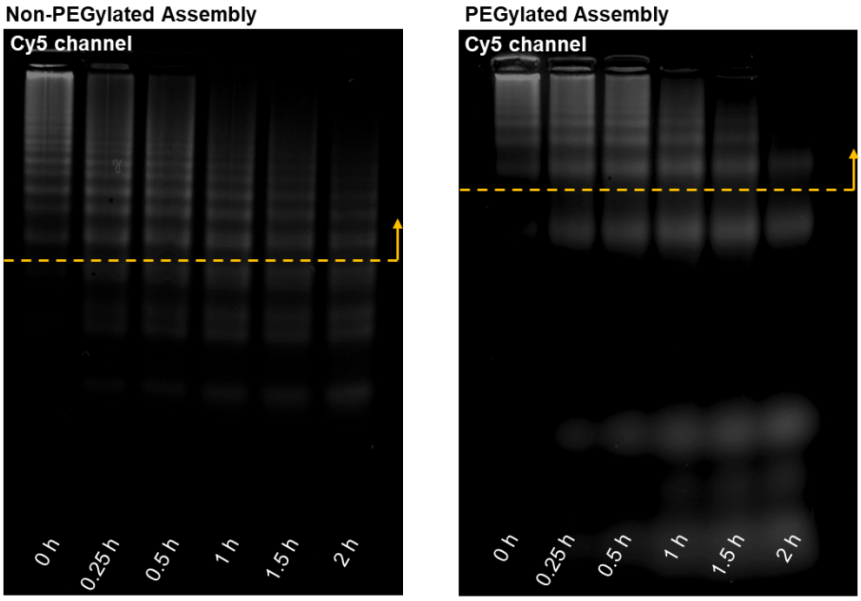

Fig. S8. AGE (5%) analysis of DNA assemblies treated with DNase I for various amounts of time (Cy5 channel). Dashed line indicates a cut-off for high molecular weight fractions (>50 kDa).

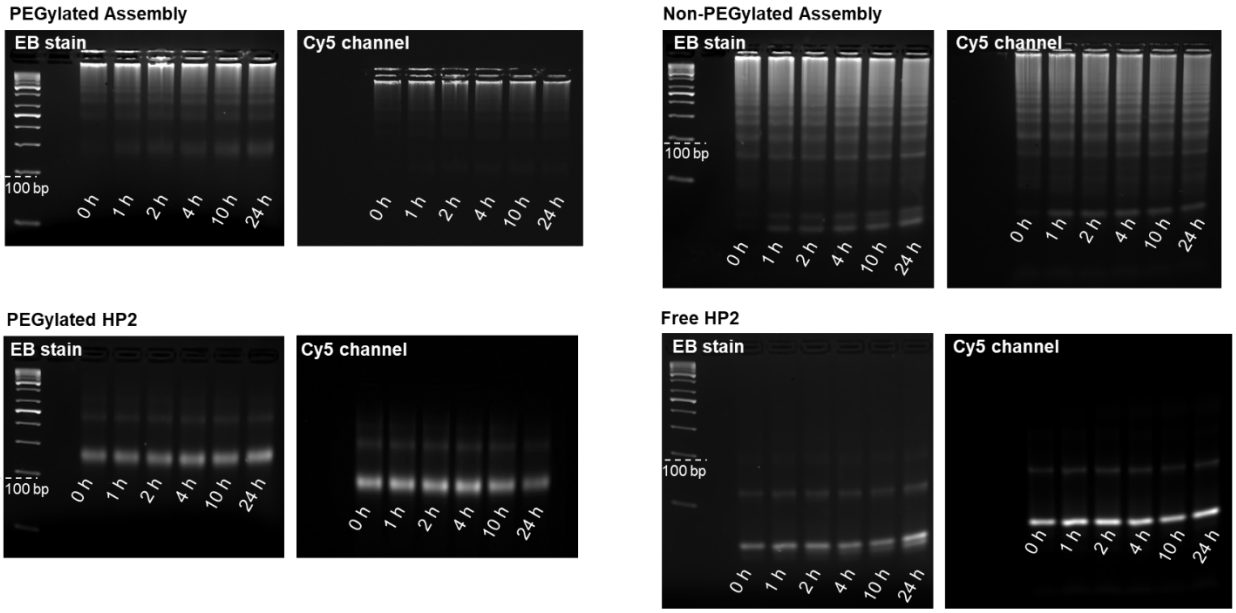

Fig. S9. AGE (5%) analysis of DNA assembly and monomers treated with full-serum RPMI medium (10% FBS) for various amounts of time up to 24 h.

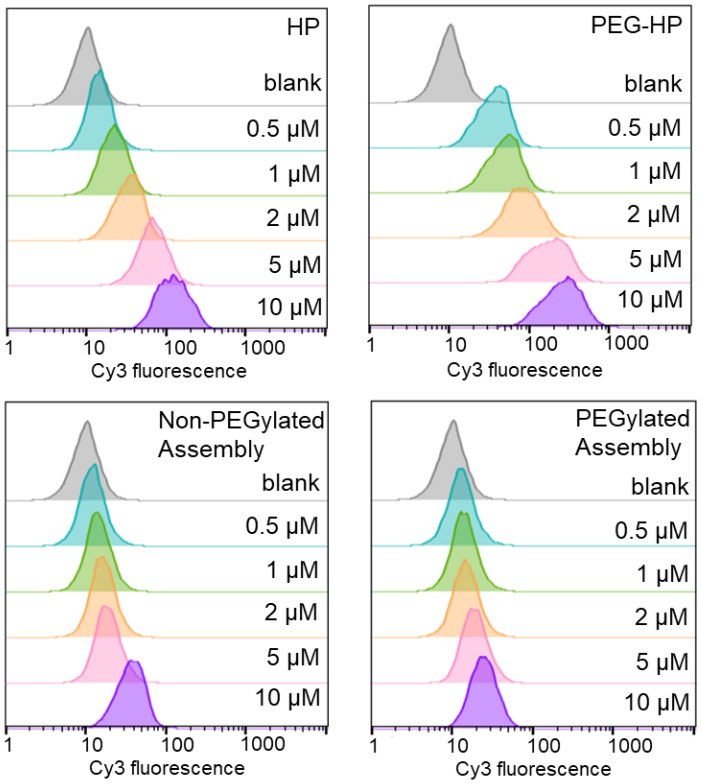

Fig. S10. Flow cytometry measurement of PC9 cells treated with DNA assemblies and their monomers.

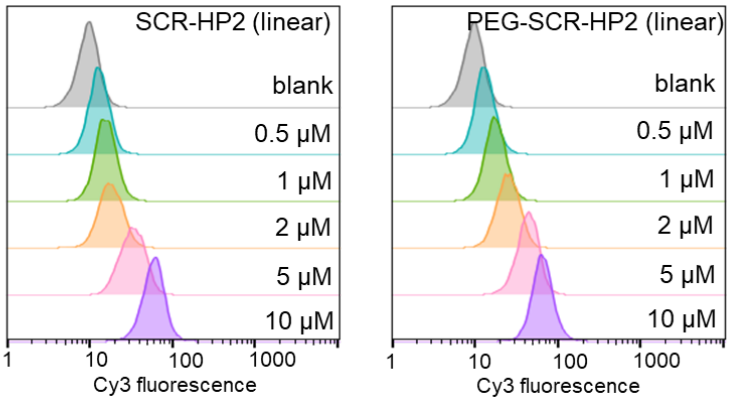

Fig. S11. Flow cytometry measurement of NCI-H358 cells treated with scramble-HP and PEGylated scramble-HP.

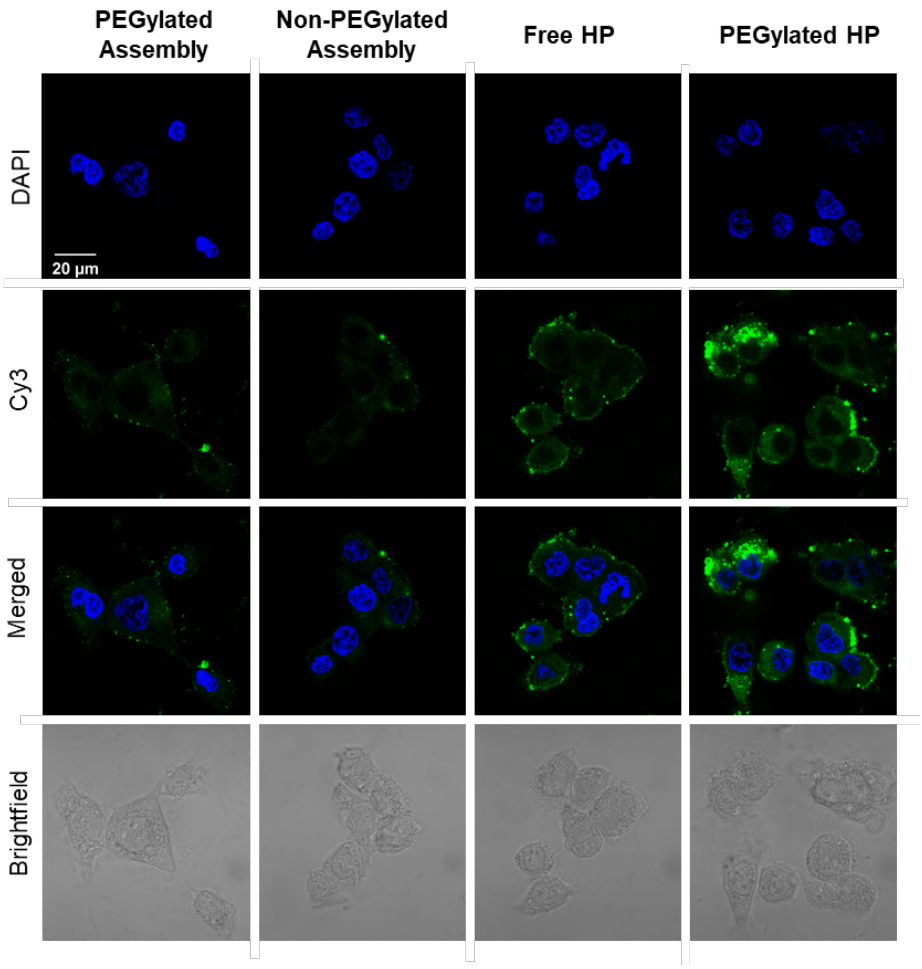

Fig. S12. Confocal microscopy images of cells treated with Cy3-labeled DNA assemblies and their precursors in serum-free RPMI medium for 24 h.

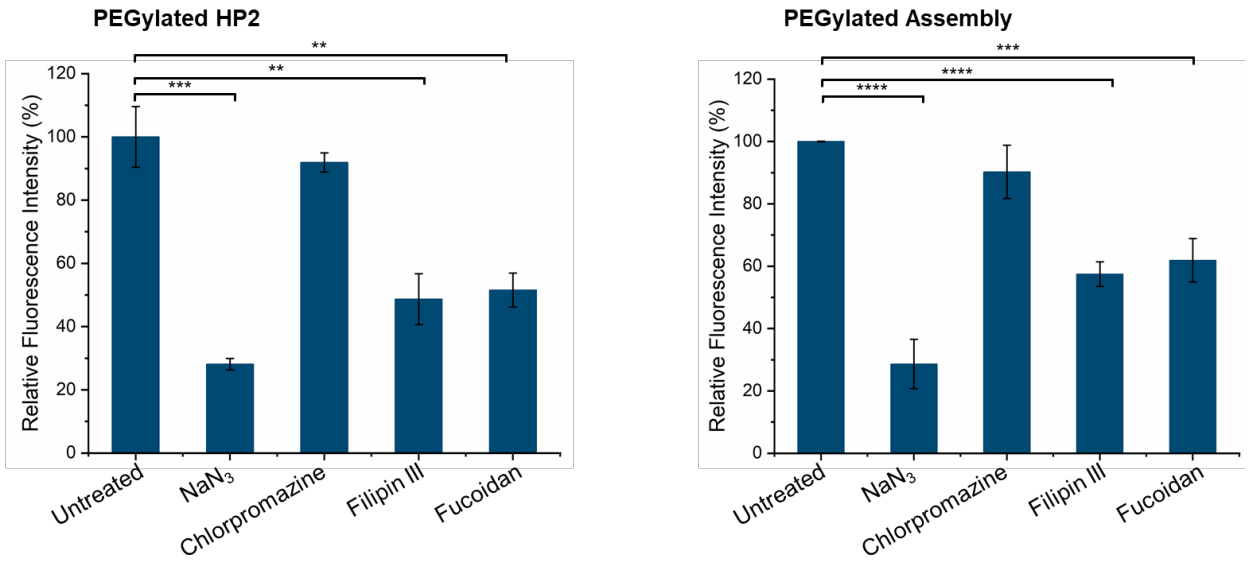

Fig. S13. Relative cellular uptake of PEGylated HP2 and PEGylated assembly in NCI-H358 cells pretreated with pharmacological inhibitors. ***P*<0.01, ****P*<0.001 *****P*<0.0001 (two-tailed test).

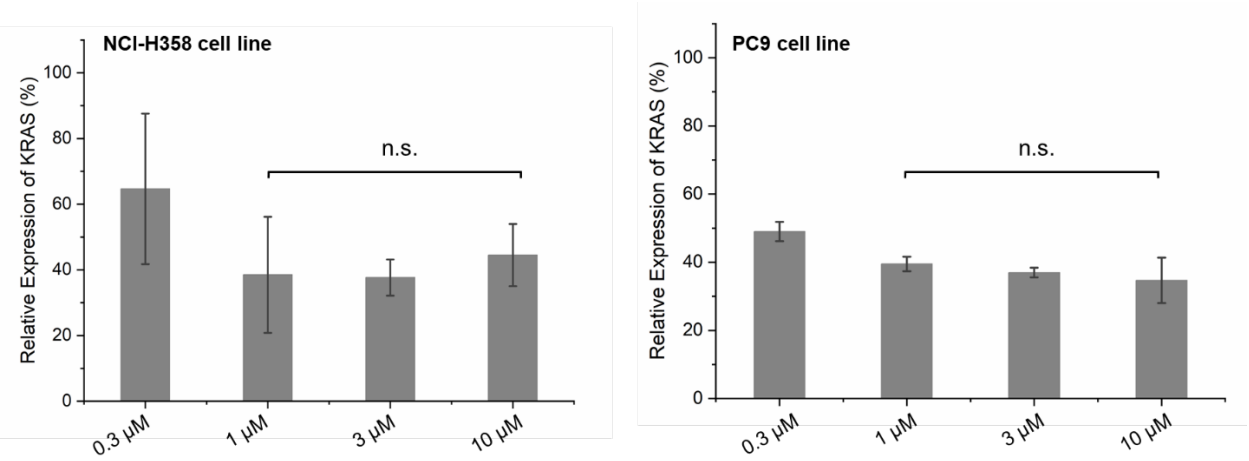

Fig. S14. KRAS knockdown (protein level) in NCI-H358 and PC9 cell lines by PEGylated assembly. Level of knockdown no longer show dosage-response beyond 1 μM of antisense strand.

1. Li, Z.; He, X.; Luo, X.; Wang, L.; Ma, N., DNA-Programmed Quantum Dot Polymerization for Ultrasensitive Molecular Imaging of Cancer Cells. Anal Chem 2016, 88 (19), 9355-9358.
2. Zadeh, J. N.; Steenberg, C. D.; Bois, J. S.; Wolfe, B. R.; Pierce, M. B.; Khan, A. R.; Dirks, R. M.; Pierce, N. A., Nupack: Analysis and Design of Nucleic Acid Systems. J Comput Chem 2011, 32 (1), 170-173.